H. B. Yin
LNM,
Institute of Mechanics,
Chinese Academy of Sciences,
Beijing 100190, China;
School of Engineering Sciences,
University of Chinese Academy of Sciences,
Beijing 100049, China

S. H. Chen[1]
Institute of Advanced Structure Technology,
Beijing Institute of Technology,
Beijing 100081, China;
Beijing Key Laboratory of Lightweight
Multi-Functional Composite
Materials and Structures,
Beijing Institute of Technology,
Beijing 100081, China
e-mail: shchen@bit.edu.cn

L. H. Liang[1]
LNM,
Institute of Mechanics,
Chinese Academy of Sciences,
Beijing 100190, China;
School of Engineering Sciences,
University of Chinese Academy of Sciences,
Beijing 100049, China
e-mail: lianglh@lnm.imech.ac.cn

Z. L. Peng
Institute of Advanced Structure Technology,
Beijing Institute of Technology,
Beijing 100081, China;
Beijing Key Laboratory of Lightweight
Multi-Functional Composite
Materials and Structures,
Beijing Institute of Technology,
Beijing 100081, China

Y. G. Wei
College of Engineering,
Peking University,
Beijing 100871, China

Quantitative Prediction of the Whole Peeling Process of an Elastic Film on a Rigid Substrate

The whole peeling behavior of thin films on substrates attract lots of research interests due to the wide application of film-substrate systems, which was well modeled theoretically by introducing Lennard–Jones (L-J) potential to describe the interface in Peng and Chen (2015, Effect of Bending Stiffness on the Peeling Behavior of an Elastic Thin Film on a Rigid Substrate," Phys. Rev. E, 91(4), p. 042401). However, it is difficult for real applications because the parameters in the L-J potential are difficult to determine experimentally. In this paper, with the help of the peeling test and combining the constitutive relation of a cohesive zone model (CZM) with the L-J potential, we establish a new method to find the parameters in the L-J potential. The whole peeling process can then be analyzed quantitatively. Both the theoretical prediction and the experimental result agree well with each other. Finite element simulations of the whole peeling process are carried out subsequently. Quantitative agreements among the theoretical prediction, numerical calculation, and the experiment measurement further demonstrate the feasibility of the method. Effects of not only the interface strength but also the interface toughness on the whole peeling behavior are analyzed. It is found that the peeling force at a peeling angle of 90 deg during the steady-state stage is affected only by the interface toughness, while the peeling force before the steady-state stage would be influenced significantly by the interface toughness, interface strength, and bending stiffness of the film. All the present results should be helpful for deep understanding and theoretical prediction of the interface behavior of film-substrate systems in real applications. [DOI: 10.1115/1.4040336]

Keywords: film-substrate system, interface behavior, peeling force, cohesive zone model, L-J potential

1 Introduction

Film-substrate systems play an important role in various industries, for example, bionic device designing, medical protection, modern material manufacturing [1–3], etc. Fundamental understanding of the peeling behavior and debonding mechanism of films should be very significant. The peel test as a well-known technique to measure the interface properties between thin films and substrates was designed by Spies [4], and such a test technique has become very popular in assessing the interface mechanical properties so far because of its easy operation [5–8]. Kendall's model [9] as a classical theory to analyze the interface behavior of an elastic film peeling from a rigid substrate has been widely accepted. As a pioneering work, Kendall's model first gives an analytical relationship between the peeling force, peeling angle, film's modulus, and interface toughness (i.e., interface adhesion energy) in the steady-state peeling stage. It should be noted that for an elastic film, Kendall' model is accurate enough to predict the peeling force in the steady-state peeling stage, so it is often used to determine the interface toughness by measuring the peeling force experimentally. The effects of film's plasticity [7,10–12], film's viscoelasticity [13,14], film's heterogeneity [15], environmental humidity [16], pretension in films [17], substrate's viscoelasticity [18], interface roughness [3,19,20], etc., on the peeling behaviors were also discussed by many researchers. In the Kendall's model, the stress distribution between films and substrates cannot be achieved and the interface toughness is the only interface parameter considered.

In order to model the peeling behavior of films more comprehensively, some interface models between films and substrates were introduced, such as the Lennard–Jones (L-J) potential [21,22] and interface cohesive zone models (CZM) [8,23,24]. Among these studies, most of them focused on the steady-state

[1]Corresponding authors.

Contributed by the Applied Mechanics Division of ASME for publication in the Journal of Applied Mechanics. Manuscript received March 8, 2018; final manuscript received May 21, 2018; published online June 14, 2018. Editor: Yonggang Huang.

peeling process and neglected the peeling behavior before the steady-state peeling stage. The steady-state peeling process requires the film's axis at the loading end strictly consistent with the direction of the external peeling force [25]. In the steady-state stage, the peeling force keeps a constant and can be expressed analytically. But in a practical peeling problem, especially for films with finite bending stiffness, the above condition is not always satisfied strictly [26]. Furthermore, many peeling experiments also show that the peeling force would vary as a function of the peeling displacement, in which the maximum peeling force may not appear at the steady-state stage but at the initial peeling stage [11,14]. Therefore, researches on the peeling behavior in the initial stage or the whole peeling process should be carried out. However, such a study on the whole peeling process or the initial peeling stage is still few. Oyharcabal and Frisch studied theoretically the whole peeling process of an elastic inextensible rod from a smooth substrate using a continuum mechanics method [21]. In their model, only the bending energy was considered and only the case of a 90 deg peeling angle was discussed. Peng and Chen further studied the effect of film's bending stiffness on the whole peeling process with an arbitrary peeling angle [22]. Both models successfully described not only the peeling behavior in the steady-state stage but also the whole peeling process with the help of the L-J potential that was used to describe the interaction between films and substrates. As we know, the L-J potential describes essentially the interaction among atoms and the related parameters in the L-J potential are difficult to determine for a real film-substrate system, though the integral of L-J potential could provide the interface interaction energy and the interaction force between films and substrates. Thus, the first question is how to obtain the parameters in the L-J potential with the help of a real peeling test. Consequently, another question is how to predict the interface peeling behavior quantitatively, which may be useful for real applications.

In order to answer the above questions, we ask the interface cohesive zone model for help, which was often introduced to describe the interface interaction [8,23,27]. Bridging the cohesive zone model and the L-J potential model, we find the relation between the parameters in L-J potential and those in the cohesive zone model. With the help of peeling test, the whole peeling behavior of a film-substrate system could be analyzed quantitatively based on the L-J potential model. Finite element calculation is further carried out in order to not only verify the method but also analyze systematically the interface effect on the whole peeling behavior.

One should be noted that for an elastic film-substrate system with a fixed interface toughness but with a very strong interface strength, the film peeling model would not be accurate enough. A beam model may be adopted. In this paper, the case with a very strong interface strength is obviously not included.

2 The Peeling Model With the Lennard–Jones Potential

Peng and Chen have established a plane strain peeling model for an elastic film-substrate system [22]. The whole peeling process including the initial stage and the steady-state stage is analyzed based on the L-J potential describing the interface interaction as shown in Fig. 1. The total potential energy Π of the film-substrate system can be expressed as

$$\Pi = \int_0^L \frac{1}{2} D\theta'^2(s)ds + \int_0^L \frac{1}{2} E\varepsilon^2 h ds - \mathbf{Pu} - \int_0^L P\varepsilon ds + \int_0^L V(y)ds \tag{1}$$

where the first term on the right-hand side of Eq. (1) is the bending elastic energy, $D = Eh^3/12$ is the bending stiffness of the film. Here, E and h denote the film's Young's modulus and thickness, respectively. The second term on the right-hand side is the

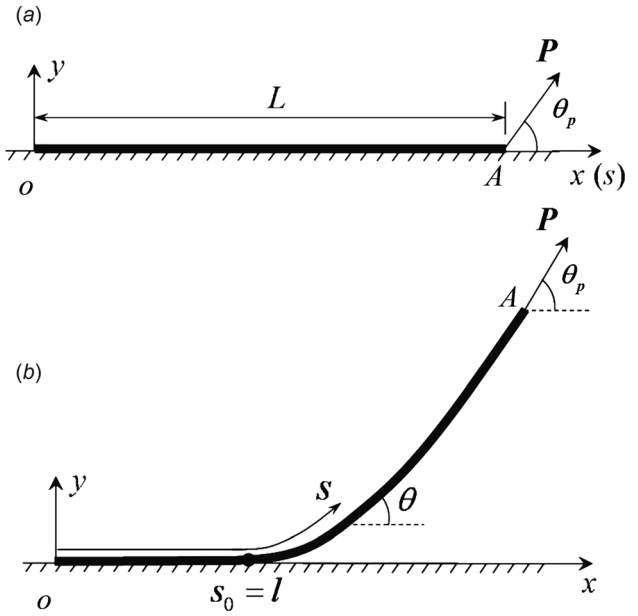

Fig. 1 Schematics of an elastic thin film with a length *L* peeling from a rigid substrate with a peeling force *P* and a peeling angle θ_P at the right end of the film. A curvilinear coordinate (s, θ) and a rectangular one (x, y) are attached to the film-substrate system with the origin *o* at the left end of the film. (*a*) The initial peeling state and (*b*) an intermediate state.

elastic strain energy stored in the elastic film. The third term is the potential of the external force due to the displacement **u** at the loading point A without considering the film's extension. The fourth term is the work done by the external force due to the tension of the elastic film. The last term is the interaction potential energy between the film and the substrate, which can be obtained based on the L-J potential

$$V(y) = \alpha\left[\left(\frac{\beta}{y}\right)^9 - \left(\frac{\beta}{y}\right)^3\right] \tag{2}$$

Here, the interface parameters α and β represent the depth of the potential well and the effective interaction distance, respectively.

The principle of the minimum potential energy yields the governing equation as

$$\begin{cases} D\dfrac{d^2\theta}{ds^2} + \lambda_1\cos\theta + \dfrac{P^2}{Eh}\cos(\theta-\theta_P)\sin(\theta-\theta_P) \\ -P\sin(\theta-\theta_P) - \dfrac{P^2}{Eh}\sin(\theta-\theta_P)\cos(\theta_L-\theta_P) = 0 \\ \dfrac{d\lambda_1}{ds} = -\dfrac{\partial V}{\partial y} \\ \dfrac{dx}{ds} = \cos\theta \\ \dfrac{dy}{ds} = \sin\theta \end{cases} \tag{3}$$

and the boundary conditions as

$$\lambda_1(L) = 0 \quad \left.\frac{d\theta}{ds}\right|_{s=0} = 0 \quad \left.\frac{d\theta}{ds}\right|_{s=L} = 0 \tag{4}$$

where λ_1 is an Lagrange multiplier, θ is the tangential angle of each point on the film, θ_L is the corresponding tangential angle of

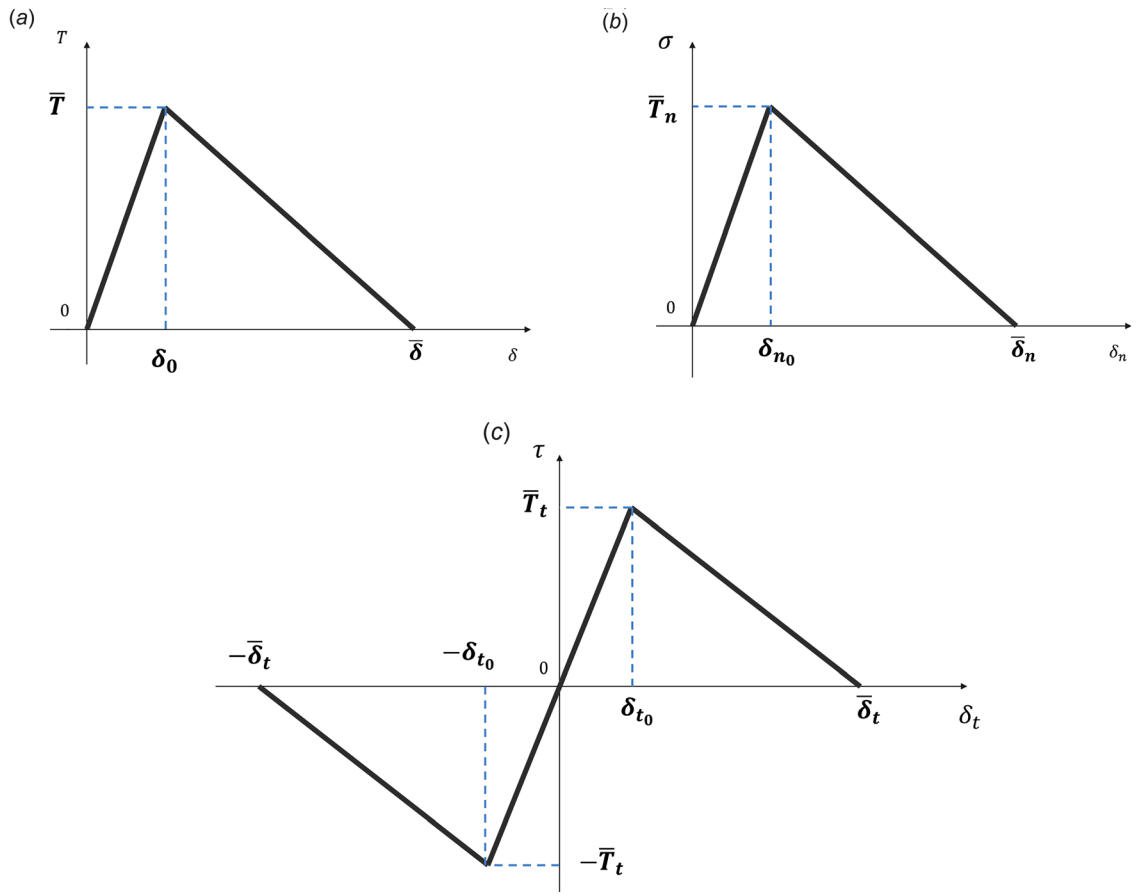

Fig. 2 The bilinear T-S curves of the interface CZM: (*a*) the total response, (*b*) the response in the normal direction, and (*c*) the response in the tangent direction

the point near the right end of the film, s is the arc length of the film from the origin o.

A standard shooting method can be used to find the peeling force P at a given moment. However, for a practical problem, quantitative analysis is often required, which needs the values of α and β to be known in advance. How to find the values of α and β based on a peeling test is still a difficult problem. Therefore, the interface cohesive zone model is introduced as follows in order to give a method to determine the interface parameters in the L-J potential.

3 The Interface Cohesive Zone Model

The interface CZM as a macroscopic and phenomenological interface model is widely used to describe interfaces [5,23,24]. The CZM constitutive equations are based on the traction-separation (T-S) relations [28,29]. In the T-S relations, the peak value of the traction and the area under the T-S curves are two key parameters [23,27,30,31], which are denoted as the interface strength and the interface toughness, respectively. The simple bilinear T-S relation as shown in Fig. 2 is widely adopted to capture the interface properties. Figure 2(*a*) represents the total traction-separation response under a mixed tension and shear loading mode. Figures 2(*b*) and 2(*c*) show the response under pure tension and pure shear, respectively. All the T-S curves have a similar shape and can be expressed as Eqs. (5)–(7), respectively,

$$T=\begin{cases}\bar{T}\dfrac{\delta}{\delta_0} & \delta\le\delta_0\\ \bar{T}\dfrac{\bar{\delta}-\delta}{\bar{\delta}-\delta_0} & \delta_0<\delta<\bar{\delta}\\ 0 & \bar{\delta}\le\delta\end{cases}\quad\text{(total response)}\qquad(5)$$

$$\sigma=\begin{cases}\bar{T}_n\dfrac{\delta_n}{\delta_{n_0}} & \delta_n\le\delta_{n_0}\\ \bar{T}_n\dfrac{\bar{\delta}_n-\delta_n}{\bar{\delta}_n-\delta_{n_0}} & \delta_{n_0}<\delta_n<\bar{\delta}_n\\ 0 & \bar{\delta}_n\le\delta_n\end{cases}\quad\text{(normal direction)}\qquad(6)$$

$$\tau=\begin{cases}0 & \delta_t\le-\bar{\delta}_t\\ \bar{T}_t\dfrac{-\bar{\delta}_t-\delta_t}{\bar{\delta}_t-\delta_{t_0}} & -\bar{\delta}_t<\delta_t<-\delta_{t_0}\\ \bar{T}_t\dfrac{\delta_t}{\delta_{t_0}} & -\delta_{t_0}\le\delta_t\le\delta_{t_0}\\ \bar{T}_t\dfrac{\bar{\delta}_t-\delta_t}{\bar{\delta}_t-\delta_{t_0}} & \delta_{t_0}<\delta_t<\bar{\delta}_t\\ 0 & \bar{\delta}_t\le\delta_t\end{cases}\quad\text{(tangent direction)}\qquad(7)$$

Here, T, σ, and τ represent the total, normal, and tangent separating stresses, respectively. δ, δ_n, and δ_t represent the separating displacements corresponding to the total, normal, and tangent separating stresses, respectively. $\bar{T}(\bar{T}_n$ or $\bar{T}_t)$ and $\bar{\delta}(\bar{\delta}_n$ or $\bar{\delta}_t)$ represent the total (normal or tangent directional) interface separating strength and the maximum interface separating displacement, respectively. δ_0, δ_{n_0}, and δ_{t_0} represent the critical separating displacements corresponding to $\bar{T}$, $\bar{T}_n$, and $\bar{T}_t$, respectively. When $\delta>0$, the area under the T-S curve is denoted as the interface toughness G_c, which is also called the interface adhesive energy

or the interface fracture energy. The interface toughness in three different loading cases can be expressed as

$$\begin{cases} G_c = \int_0^{\bar{\delta}} T d\delta = \frac{1}{2}\bar{T}\bar{\delta} & \text{(total response)} \\ G_{nc} = \int_0^{\bar{\delta}_n} \sigma d\delta_n = \frac{1}{2}\bar{T}_n\bar{\delta}_n & \text{(normal direction)} \\ G_{tc} = \int_0^{\bar{\delta}_t} \sigma d\delta_t = \frac{1}{2}\bar{T}_t\bar{\delta}_t & \text{(tangent direction)} \end{cases} \tag{8}$$

Under a mixed loading, we have $\delta = \sqrt{\langle\delta_n\rangle^2 + \delta_t^2}$. When the load increases beyond the critical value, the interface begins to soften. At this time, we have

$$\text{MAX}\left\{\frac{\langle\sigma\rangle}{\bar{T}_n}, \frac{\tau}{\bar{T}_t}\right\} = 1 \tag{9}$$

Here, $\langle\rangle$ represents the Macaulay bracket defined as $\langle x\rangle = (|x| + x)/2$, which means that a compressive deformation or stress state does not induce interface separation. With an increasing interface separating displacement, interface debonding would happen at $\delta = \bar{\delta}$. At this moment, we have

$$\frac{G_n}{G_{nc}} + \frac{G_t}{G_{tc}} = 1 \tag{10}$$

Here, G_n and G_t represent the work done by the traction in the normal and the shear directions, respectively. G_{nc} and G_{tc} are the interface toughness defined in Eq. (8). When Eq. (10) is satisfied, the interface roughness is $G_c = G_n + G_t$. In this paper, the simple bilinear separation law in Eq. (5) is used, in which the tension and shear directions are coupled through the mixed-mode failure criterion in Eq. (10).

The effect of the stiffness of the cohesive element on the peeling behavior is investigated first. The results demonstrate an insensitive effect in cases with a 90 deg peeling angle. Therefore, the prediction in cases with a 90 deg peeling angle based on the CZM is dependent only on two characteristic parameters, i.e., the interface strength ($\bar{T}$) and the interface toughness (G_c) [5,24,31], the fact of which will be well adopted in the following analysis.

4 Determination of the Interface Parameters in the Lennard–Jones Potential

The first-order derivative of the L-J potential energy in Eq. (2) with respect to y corresponds to the interface traction force

$$V'(y) = \frac{\alpha}{\beta}\left[-9\left(\frac{\beta}{y}\right)^{10} + 3\left(\frac{\beta}{y}\right)^{4}\right] \tag{11}$$

The traction-separation curve of Eq. (11) is shown in Fig. 3 with a peak value of the traction $0.47\alpha/\beta$ and an area under the curve 0.384α, both of which represent the interface strength and the interface roughness in the L-J potential form, respectively.

Comparing the bilinear T-S curve in Fig. 2(*a*) and the T-S relation of the L-J potential form in Fig. 3, both curves have a similar shape. Since the peak value of the traction (i.e., the interface strength) and the area under the curve (i.e., the interface toughness) are two dominant parameters in the T-S relations, let the two parameters in the two models equal each other, i.e.,

$$\begin{cases} \bar{T} = 0.47\dfrac{\alpha}{\beta} \\ G_c = 0.384\alpha \end{cases} \tag{12}$$

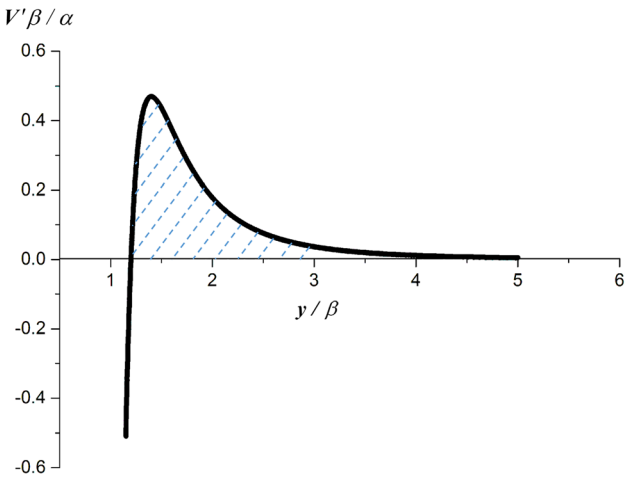

Fig. 3 The T-S curve of the L-J potential, where y/β is the dimensionless interface separation displacement and $V'\beta/\alpha$ is the dimensionless interface traction

which yields

$$\begin{cases} \alpha = 2.604G_c \\ \beta = 1.22\dfrac{G_c}{\bar{T}} \end{cases} \tag{13}$$

Here, one can note that if the parameters G_c and $\bar{T}$ of an interface in real applications are known, the corresponding parameters α and β in the L-J potential can be achieved easily. Then, the whole peeling process of a thin film on a substrate can be analyzed quantitatively by solving Eqs. (3) and (4). In order to verify the proposed method above and analyze the effects of interface and other parameters on the whole peeling behavior of film-substrate system, peeling tests are carried out as follows.

5 Peeling Test of Film-Substrate Systems

5.1 Specimen Preparation. A series of films with different thickness are prepared. Each film consists of two layers, in which the upper layer is polyvinylchloride (PVC) plate and the bottom layer is 3 M Vinyl Electrical Tape (3 M #1500). The 3 M Vinyl Electrical Tape is also mainly made of PVC so that two layers have very similar mechanical properties. The thickness of the bottom layer is fixed, on which the upper layer with different thickness is bonded in order to change the total thickness of PVC films but possess an unchanged property of the bottom surface. The width of the upper and bottom layers keeps the same. The cyanoacrylate glue (502 glue) is used to bond both layers.

Two substrates, i.e., PVC and glass, are adopted to bond with the same films to achieve different interface properties. The schematic of the film/substrate specimen is shown in Fig. 4. The width b of the film is 18 mm. Films with different thickness h are used, i.e., 0.4 mm, 0.6 mm, and 0.7 mm, respectively.

Before bonding the film to the substrate, the surface of the substrate is carefully cleaned with absolute ethyl alcohol and then rinsed with distill water. After bonding, a hand roll is used to roll the film on the substrate in both directions, in order to achieve a nearly perfect adhesion interface and avoid air bubbles entrapped in the interface. Finally, before the peeling test, the specimens are placed in the room temperature (about 25 °C) environment for about 4 h.

5.2 Peeling Experiment. As shown in Fig. 5, all the experiments are conducted using a universal test machine (Instron 2367B11466). Before the experiment, the specimen is fixed to a peeling fixture, which is specially designed for the peeling test. The fixture is made of four parts, a slide rail, a slide platform, a

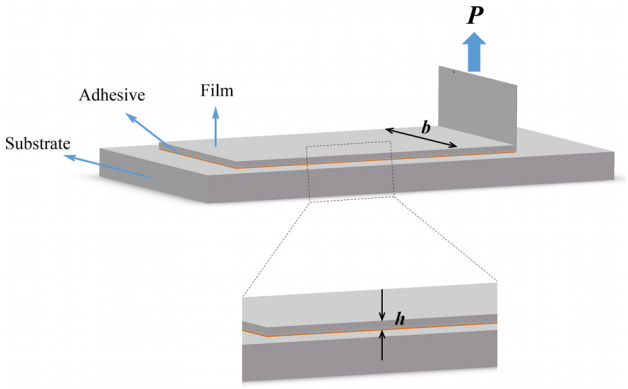

Fig. 4 Schematic of the peeling test

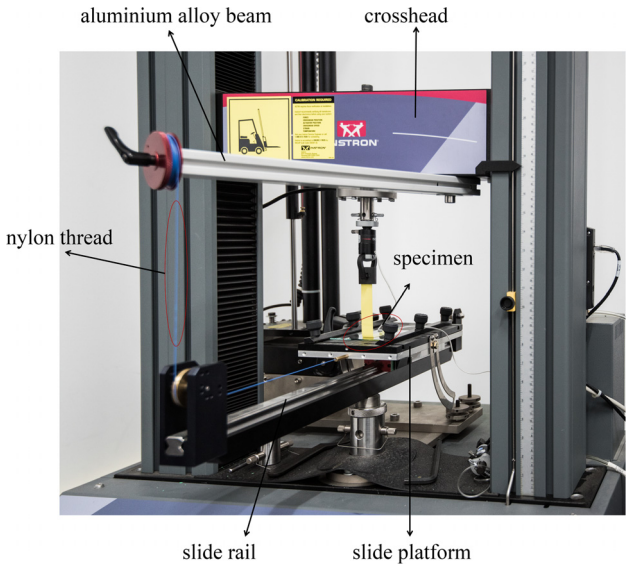

Fig. 5 The universal test machine and the peeling fixture

nylon thread, and an aluminum alloy beam. One side of the aluminum alloy beam is fixed to the crosshead of the universal test machine. The other side is connected to the slide platform using the nylon thread, which goes through a pulley fixed at the edge of the slide rail. Using such a technique, the peeling angle can remain invariable during the peeling test, because the movement of the peeling tip will be offset by the platform with the same displacement but in an opposite direction. The moving speed of the crosshead is set as 10 mm/min so that the viscoelastic effect can be neglected in the experiment. Clear pictures of the interface cohesive zone are captured by a CCD (Genie Nano) with a zoom lens (1–6.3 times).

Experiment of the peeling angle of 90 deg is only carried out in this paper since the interface toughness can be directly found from the peeling force in the steady-state stage. Then, through Eq. (13), we can find the parameters α and β in the L-J potential.

5.3 Experimental Results. Figures 6(*a*) and 6(*b*) show the peeling force–displacement curves of films with different thickness on a PVC substrate and a glass substrate, respectively. For each film, the peeling force increases initially up to a peak value, then decreases gradually before reaching a steady-state platform. The peak value and the value of the steady-state platform correspond to the maximum peeling force and the steady-state peeling force, respectively. It can be found that the steady-state peeling force is almost the same for different films on the same substrate. It is because that all the film/substrate systems possess a very similar interface and the steady-state peeling force is only related to interface properties, which agrees well with the prediction of the Kendall's model [9]. The steady-state peeling force of the film/PVC systems as shown in Fig. 6(*a*) is larger than that of the film/glass systems as shown in Fig. 6(*b*), which is due to the stronger interface toughness between the film and the PVC substrate. Furthermore, the maximum peeling force is found to increase with an increasing film's thickness, which is consistent with the theoretical prediction of Peng and Chen's model [22]. It is mainly because the maximum peeling force emerges at the initial peeling stage and the effect of bending stiffness of films should be considered at the initial stage.

The interface cohesive zone can be clearly captured during the tests as shown in Figs. 7(*a*) and 7(*b*) for the PVC substrate case and the glass substrate case, respectively. The maximum separating displacement $\bar{\delta}$ can be precisely measured from Fig. 7, which is 1.2 mm and 0.7 mm for the PVC substrate and glass

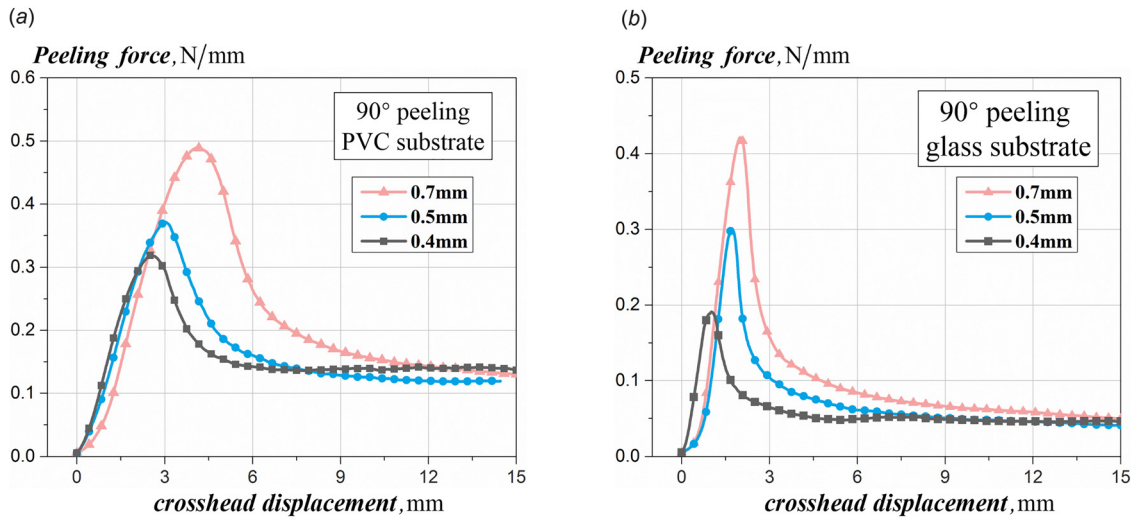

Fig. 6 The peeling force-crosshead displacement curves with films of different thickness on different substrates in the case with the peeling angle of 90 deg: (*a*) the experimental data on PVC substrates and (*b*) the experimental data on glass substrates

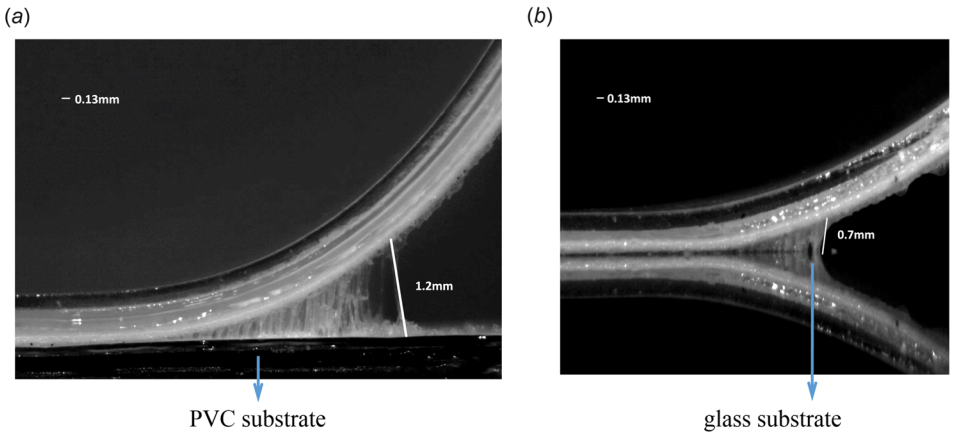

Fig. 7 Pictures of the cohesive zone for different substrate interfaces: (*a*) the interface of a film on a PVC substrate and (*b*) the interface of a film on a glass substrate

substrate, respectively. It should be noted that the mirror picture of the interface cohesive zone is also exhibited in Fig. 7(*b*) due to the glass substrate.

6 Comparison Between the Experimental Results and the Extended Peng and Chen's Model

Combining the experimental measurement and the Peng and Chen's model could carry out the quantitative verification of Eq. (13). The theoretical results can be obtained based on Eqs. (1)–(4). The parameters of the film, including the thickness and modulus, can be obtained easily from the experiments. For the PVC film, the modulus is $E_f = 1000\,\text{MPa}$. According to the Kendall's model, when the peeling angle is 90 deg, the steady-state peeling force approximately equals the interface toughness, i.e., $G_c \approx P$. From the experiment results of the PVC substrate, the interface toughness and the maximum separating displacement can be achieved as $G_c = 0.13\,\text{mJ/mm}^2$ and $\bar{\delta} = 1.2\,\text{mm}$ as shown in Figs. 6(*a*) and 7(*a*), respectively. As for the glass substrate case, the interface toughness and the maximum separating displacement are $G_c = 0.045\,\text{mJ/mm}^2$ and $\bar{\delta} = 0.7\,\text{mm}$ as shown in Figs. 6(*b*) and 7(*b*), respectively. According to Eq. (8), the interface strength $\bar{T}$ can be calculated as

$$\bar{T} = \frac{2G_c}{\bar{\delta}} \tag{14}$$

which results in $\bar{T}$ to be 0.22 MPa and 0.13 MPa for the PVC and glass cases, respectively.

According to Eq. (13), the parameters in the L-J potential model can be obtained as $\alpha = 0.338\,\text{mJ/mm}^2$ and $\beta = 0.72\,\text{mm}$ for the PVC substrate case, and $\alpha = 0.117\,\text{mJ/mm}^2$, and $\beta = 0.42\,\text{mm}$ for the glass substrate case. Substituting the corresponding values into the Peng and Chen's model, quantitatively theoretical results can be yielded as shown in Fig. 8, where the experimental measurements are also given for comparison. It can be found that not only the maximum peeling force but also the steady-state peeling force is well consistent with each other. It means the theoretical model based on the L-J potential [19] can be used to predict the whole peeling process quantitatively when the interface cohesive zone model is adopted to find the parameters in the L-J potential. One may note that the stiffness of the curves in the experimental measurement deviates from the theoretical prediction. It is mainly due to the existing free and relaxed type attached at the end of the film before the peeling experiment, which would decrease the stiffness of the experimental measurement.

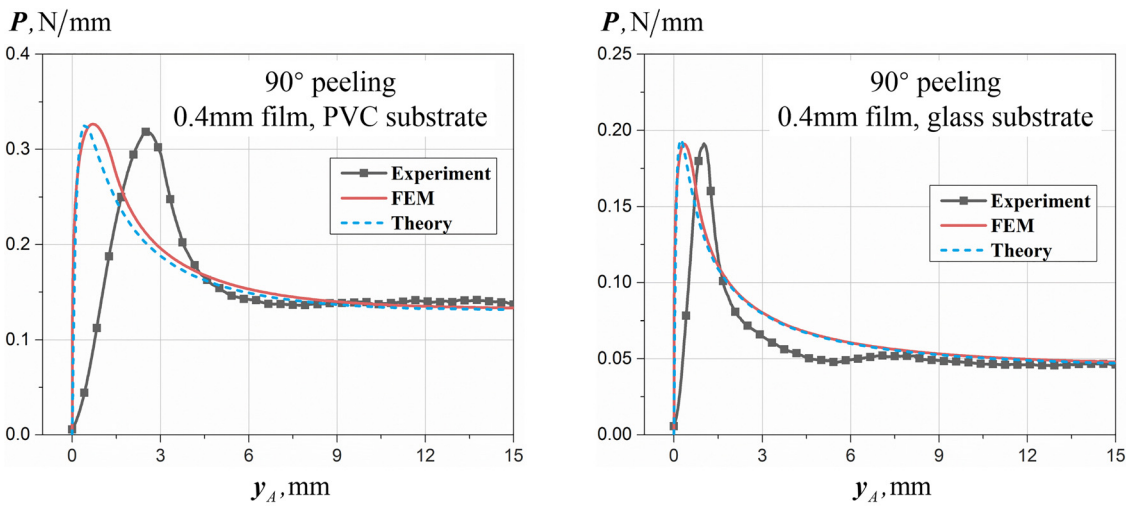

Fig. 8 Comparison of the theoretical results predicted by Peng and Chen's model [19], the finite element calculations and the experiment data in the case with the peeling angle of 90 deg: (*a*) a 0.4 mm film on a PVC substrate and (*b*) a 0.4 mm film on a glass substrate

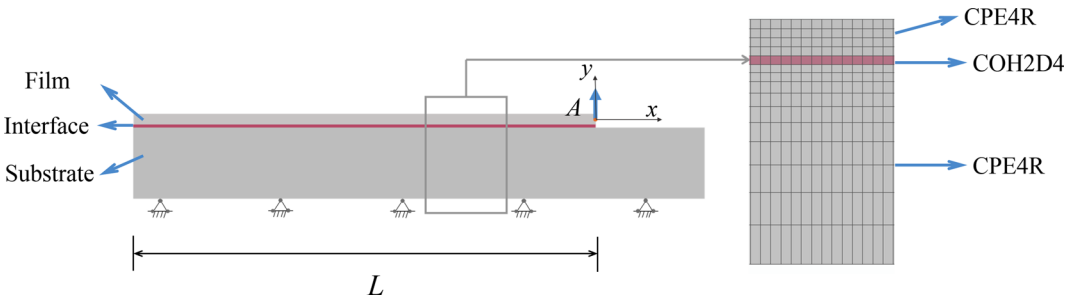

Fig. 9 The finite element model and the details of the meshes

7 Finite Element Calculation of a Film Peeling From a Substrate

7.1 Finite Element Model and Comparison of the Results. The whole peeling process of an elastic film on a rigid substrate is further simulated by a finite element model as shown in Fig. 9, in which the interface cohesive zone model is adopted to describe the interface interaction. h is the thickness of the film, L is the length of film. The bottom of the rigid substrate was fixed. Four-node rectangular elements are employed in finite element mesh, CPE4R (plane strain) elements are used for the film, COH2D4 (cohesive) elements are used for the interface layer.

Similar to the peeling test in the present paper and also due to the reason that only the vertical interaction of the interface was considered in Peng and Chen [19] by the L-J potential as shown in Eq. (2), the case with the peeling angle of 90 deg is considered in the numerical calculations.

The film is assumed to be a homogeneous, isotropic, and elastic material. Considering the plane strain condition, the constitutive equations can be written as

$$\varepsilon_{13} = \varepsilon_{31} = \varepsilon_{23} = \varepsilon_{32} = \varepsilon_{33} = 0 \tag{15}$$

$$\sigma_{ij} = \frac{E_f \nu_f}{(1-2\nu_f)(1+\nu_f)}\varepsilon_{kk}\delta_{ij} + \frac{E_f}{(1+\nu_f)}\varepsilon_{ij} \quad \text{(film)} \tag{16}$$

$$\sigma_{ij} = \frac{E_s \nu_f}{(1-2\nu_s)(1+\nu_s)}\varepsilon_{kk}\delta_{ij} + \frac{E_s}{(1+\nu_s)}\varepsilon_{ij} \quad \text{(substrate)} \tag{17}$$

where $\boldsymbol{\sigma}$ and $\boldsymbol{\varepsilon}$ represent the stress and strain tensors, respectively. ν and E represent the Poisson's ratio and the Young's modulus, respectively. δ_{ij} is the Kronecker delta. The subscripts f and s represent the film and the substrate, respectively. The subscripts i and j take values from 1, 2, and 3 to represent the x, y and z axis. The bilinear T-S relation in Sec. 3.1 is chosen as the constitutive relation of the interface cohesive zone model. The interface is assumed to be isotropic so that we have $\bar{T}_n = \bar{T}_t$ and $G_c = G_{nc} = G_{tc}$. The detailed parameter values keep the same as those in Sec. 5. The stiffness K in the interface cohesive model is the slope of the initial segment of the T-S curve, which is taken as $\bar{\delta}/\delta_0 = 4$. Actually, it is found that the whole response of the film-substrate system is insensitive to the value of $\bar{\delta}/\delta_0$ as shown in Fig. 10, which further supports the conclusion that the interface strength ($\bar{T}$) and the interface toughness (G_c) are two dominant parameters in the cohesive zone model [20,24].

During the peeling process, the vertical displacement y_A at the point A gradually increases. The simulation result is also shown in Fig. 8. It can be found that the whole peeling force–displacement curve is almost in agreement with the theoretical result based on the Peng and Chen's model with the help of the relation in Eq. (13).

7.2 Effect of Parameters on the Peeling Behavior. The finite element model is further used to study the effect of the interface and film's parameters on the whole peeling behavior. One should be noted that only the case with the peeling angle of 90 deg is analyzed because the steady-state peeling force approximately equals the interface toughness, i.e., $G_c \approx P$, only under this condition.

The peeling force P can be written as a function of some independent parameters through the dimension analysis

$$\frac{P}{G_c^0} = f\left(\frac{G_c}{G_c^0}, \frac{\bar{T}}{G_c^0 L}, \frac{E_f}{G_c^0 L}, \frac{h}{L}, \frac{y_A}{L}\right) \tag{18}$$

where G_c^0 is a referenced interface toughness. y_A is the vertical displacement at the point A. L is the whole length of the film as shown in Fig. 9.

The effect of the interface toughness G_c, interface strength $\bar{T}$, film modulus E_f, and film thickness h on the peeling force is shown in Figs. 11(*a*)–11(*d*), respectively. From Fig. 11, one can see that during the whole peeling process, the peeling force always increases to a peak value, then decreases, and finally keeps invariant in most of the cases. When the interface toughness is relative large, e.g., G_c is four times of the referenced value as shown in Fig. 11(*a*), the peeling force increases first at the initial peeling stage and then goes directly to the steady-state stage without a decreasing process. Such a phenomenon was also found by Peng and Chen [19], in which the effect of film's bending stiffness on the peeling force was mainly investigated. If the film's stiffness is relatively small, the peeling force would increase till the steady-state stage. Here, it is found that the similar varying trend of the peeling force-displacement relation would happen if the interface toughness is relatively large.

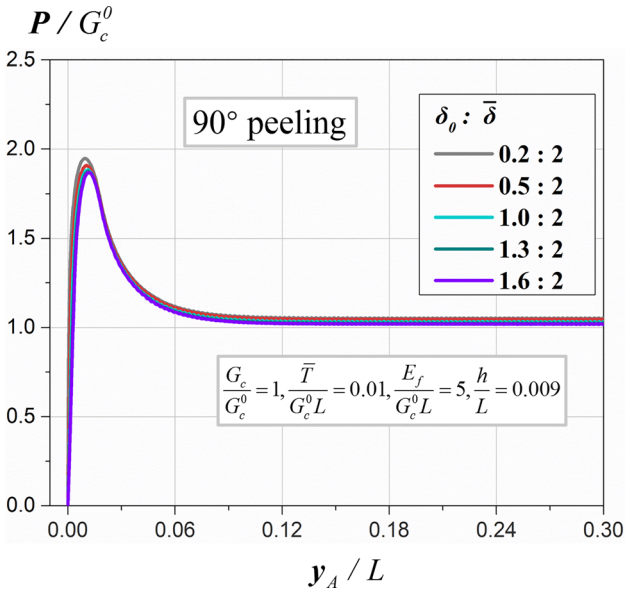

Fig. 10 The effect of the stiffness K (i.e., $\delta_0/\bar{\delta}$) in the CZM on the whole peeling behavior when the peeling angle is 90 deg

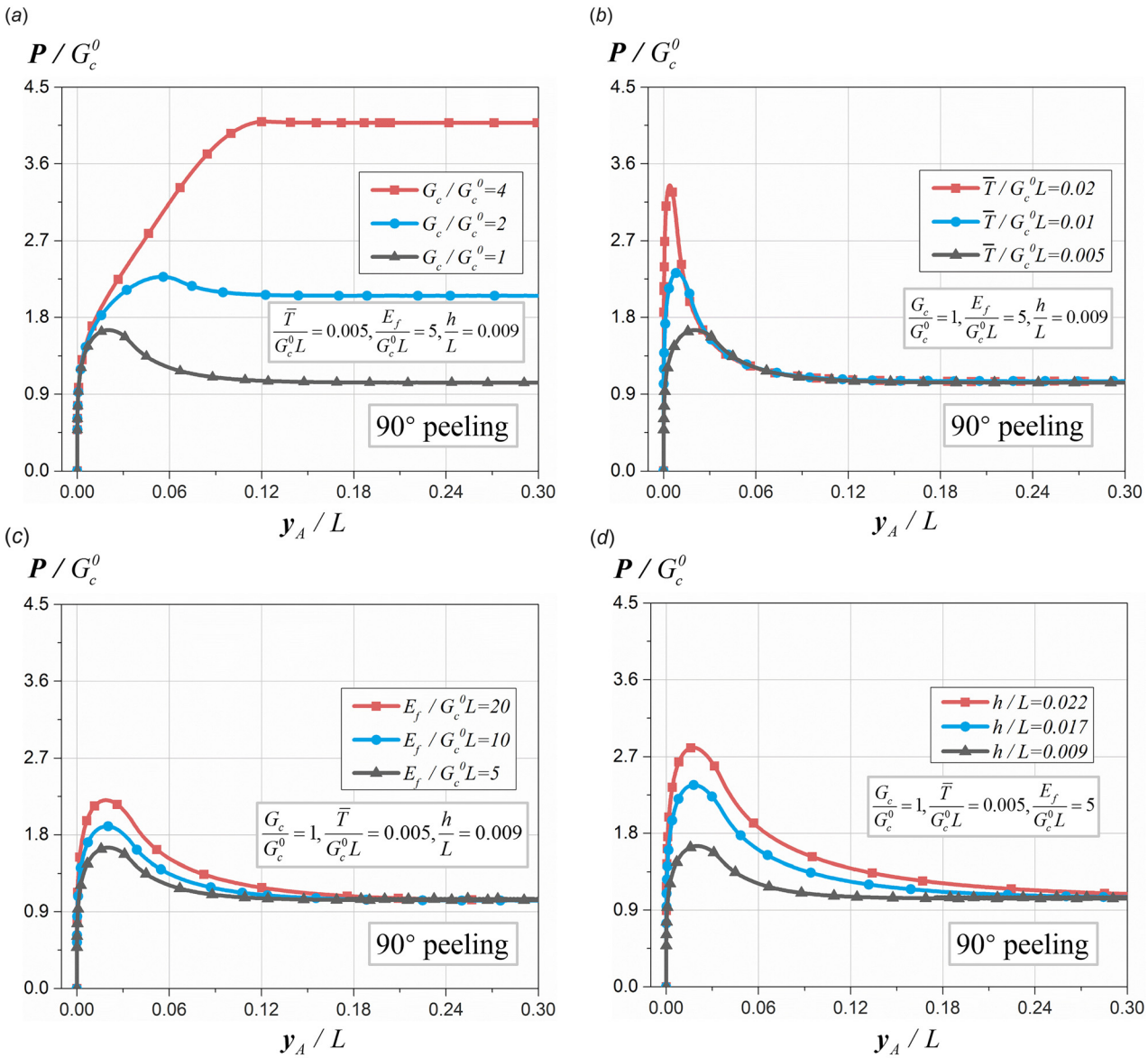

Fig. 11 The results of finite element model discussing the effect of different parameters on the peeling force in the whole peeling process in the case with the peeling angle of 90 deg: (*a*) the effect of the interface toughness, (*b*) the effect of the interface strength, (*c*) the effect of the film modulus, and (*d*) the effect of the film thickness

In addition, when the other parameters remain unchanged, the interface toughness would influence significantly not only on the peeling force at the steady-state stage but also on the peeling force during the whole peeling stage as shown in Fig. 11(*a*). However, if the interface toughness keeps unchanged and the other parameters change, the steady-state peeling force remains a constant, but the peeling process before the steady-state stage is influenced obviously by the other parameters, for example, the interface strength, the modulus, and the thickness of the film as shown in Figs. 11(*b*)–11(*d*), respectively. Comparing the theoretical results in Peng and Chen [19] shows that not only the stiffness of films but also the interface strength would show influence on the maximum peeling force, which often emerges before the steady-state stage.

Overall, the maximum peeling force would increase with the increase of the interface toughness, the interface strength, the film's modulus, and thickness, respectively. While the peeling force at the steady-state stage depends only on the interface toughness, which is consistent with the classical Kendall's model.

The maximum peeling force versus different dimensionless parameters is further shown in Fig. 12, where G_c^0, $\bar{T}^0$, E_f^0, and h^0 are the referenced interface toughness, interface strength, film modulus, and film thickness, $P_{\max}^0$ is the corresponding maximum peeling force based on the referenced parameters. It shows that the dimensionless maximum peeling force increases with the increase of different dimensionless parameters. Comparing the slope of different curves demonstrates that the effect of film thickness on the maximum peeling force is more obvious than that of the interface strength and the film modulus. The effect of the interface toughness on the maximum peeling force is less than that of the interface strength when both dimensionless parameters are relatively small. However, after the intersection point of the two curves, the effect of the interface toughness on the maximum peeling force will be much larger than that of the interface strength. Such a result should be reasonable if we check the effect of the interface toughness on the maximum peeling force as shown in Fig. 10(*a*). It shows that when the interface toughness is relatively large, the maximum peeling force will equal the peeling force at the steady-state peeling process.

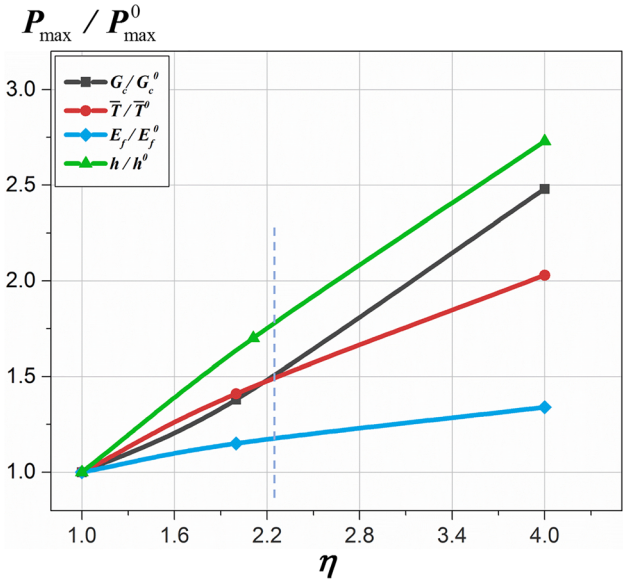

Fig. 12 The effect of different dimensionless parameters on the maximum peeling force, including the dimensionless interface toughness, interface strength, film thickness, and film's Young's modulus

One may note that only the case with the peeling angle of 90 deg is investigated due to the requirement of $G_c \approx P$. Actually, the achieved parameters α and β in the L-J potential from the peeling test of 90 deg are also true for further theoretical analysis in the other peeling angle cases. However, due to the reason that only the vertical interaction of interface was considered in the L-J potential in Ref. [19], comparison among the experimental measurement, the numerical calculation, and the theoretical result in the case with a nonvertical peeling angle further requires y in Eq. (2) to be replaced by $z = \sqrt{x^2 + y^2}$. It will be our future work.

8 Conclusion

For practical applications, the peeling model of Peng and Chen [19] based on the L-J potential is extended with the help of the interface cohesive zone model. A special relation among the parameters in the L-J potential, the interface strength, and toughness is established. All the parameters in the L-J potential can be determined by combining the special relation and the peeling test of 90 deg. Theoretical results of the whole peeling process can be achieved quantitatively, which agree well with not only the experiment measurement but also on the finite element calculation. Further numerical calculation shows that in the case with the peeling angle of 90 deg, the peeling force at the steady-state stage depends only on the interface toughness, while the interface toughness, the interface strength, the bending stiffness of the film would influence the peeling force before the steady-state stage. The present results should be helpful for deep understanding of the interface behaviors and novel design of film-substrate systems in real applications

Funding Data

- BIT Creative Research Plan.
- National Natural Science Foundation of China (Grant Nos. 11672296, 11372318, and 11532013).

References

[1] Padture, N. P., Gell, M., and Jordan, E. H., 2002, "Thermal Barrier Coatings for Gas-Turbine Engine Applications," Science, **296**(5566), pp. 280–284.
[2] Carlson, A., Bowen, A. M., Huang, Y., Nuzzo, R. G., and Rogers, J. A., 2012, "Transfer Printing Techniques for Materials Assembly and Micro/Nanodevice Fabrication," Adv. Mater., **24**(39), pp. 5284–5318.
[3] Persson, B. N. J., and Gorb, S., 2003, "The Effect of Surface Roughness on the Adhesion of Elastic Plates With Application to Biological Systems," J. Chem. Phys., **119**(21), pp. 11437–11444.
[4] Spies, G., 1953, "The Peeling Test on Redux-Bonded Joints: A Theoretical Analysis of the Test Devised by Aero Research Limited," Aircr. Eng. Aerosp. Technol., **25**(3), pp. 64–70.
[5] Wei, Y., 2004, "Modeling Nonlinear Peeling of Ductile Thin Films—Critical Assessment of Analytical Bending Models Using FE Simulations," Int. J. Solids Struct., **41**(18–19), pp. 5087–5104.
[6] Williams, J. G., 1993, "Root Rotation and Plastic Work Effects in the Peel Test," J. Adhes., **41**(1–4), pp. 225–239.
[7] Wei, Y., and Zhao, H., 2008, "Peeling Experiments of Ductile Thin Films Along Ceramic Substrates—Critical Assessment of Analytical Models," Int. J. Solids Struct., **45**(13), pp. 3779–3792.
[8] Zhao, H., and Wei, Y., 2007, "Determination of Interface Properties Between Micron-Thick Metal Film and Ceramic Substrate Using Peel Test," Int. J. Fract., **144**(2), pp. 103–112.
[9] Kendall, K., 1975, "Thin-Film Peeling-the Elastic Term," J. Phys. D, **8**(13), p. 1449.
[10] Wei, Y., and Hutchinson, J. W., 1998, "Interface Strength, Work of Adhesion and Plasticity in the Peel Test," Int. J. Fract., **93**(1), p. 315.
[11] Kim, J., Kim, K. S., and Kim, Y. H., 1989, "Mechanical Effects in Peel Adhesion Test," J. Adhes. Sci. Technol., **3**(1), pp. 175–187.
[12] Yang, Q. D., Thouless, M. D., and Ward, S. M., 1999, "Numerical Simulations of Adhesively-Bonded Beams Failing With Extensive Plastic Deformation," J. Mech. Phys. Solids, **47**(6), pp. 1337–1353.
[13] Cheng, H., 2013, "A Viscoelastic Model for the Rate Effect in Transfer Printing," ASME J. Appl. Mech., **80**(4), pp. 369–384.
[14] Peng, Z., Wang, C., Chen, L., and Chen, S., 2014, "Peeling Behavior of a Viscoelastic Thin-Film on a Rigid Substrate," Int. J. Solids Struct., **51**(25–26), pp. 4596–4603.
[15] Xia, S. M., Ponson, L., Ravichandran, G., and Bhattacharya, K., 2013, "Adhesion of Heterogeneous Thin Films—I: Elastic Heterogeneity," J. Mech. Phys. Solids, **61**(3), pp. 838–851.
[16] Peng, Z., Wang, C., Yang, Y., and Chen, S., 2016, "Effect of Relative Humidity on the Peeling Behavior of a Thin Film on a Rigid Substrate," Phys. Rev. E, **94**(3–1), p. 032801.
[17] Peng, Z., and Chen, S., 2012, "Effect of Pre-Tension on the Peeling Behavior of a Bio-Inspired Nano-Film and a Hierarchical Adhesive Structure," Appl. Phys. Lett., **101**(16), p. 163702.
[18] Afferrante, L., and Carbone, G., 2016, "The Ultratough Peeling of Elastic Tapes From Viscoelastic Substrates," J. Mech. Phys. Solids, **96**, pp. 223–234.
[19] Peng, Z. L., and Chen, S. H., 2011, "Effects of Surface Roughness and Film Thickness on the Adhesion of a Bioinspired Nanofilm," Phys. Rev. E, **83**(5), p. 051915.
[20] Chen, H., Feng, X., Huang, Y., Huang, Y., and Rogers, J. A., 2013, "Experiments and Viscoelastic Analysis of Peel Test With Patterned Strips for Applications to Transfer Printing," J. Mech. Phys. Solids, **61**(8), pp. 1737–1752.
[21] Oyharcabal, X., and Frisch, T., 2005, "Peeling Off an Elastica From a Smooth Attractive Substrate," Phys. Rev. E, **71**(3), p. 036611.
[22] Peng, Z., and Chen, S., 2015, "Effect of Bending Stiffness on the Peeling Behavior of an Elastic Thin Film on a Rigid Substrate," Phys. Rev. E, **91**(4), p. 042401.
[23] Liang, L. H., Wei, H., Li, X. N., and Wei, Y. G., 2013, "Size-Dependent Interface Adhesive Energy and Interface Strength of Nanostructured Systems," Surf. Coat. Technol., **236**(2), pp. 525–530.
[24] Li, X. N., Liang, L. H., Xie, J. J., Chen, L., and Wei, Y. G., 2014, "Thickness-Dependent Fracture Characteristics of Ceramic Coatings Bonded on the Alloy Substrates," Surf. Coat. Technol., **258**, pp. 1039–1047.
[25] Sauer, R. A., and Wriggers, P., 2009, "Formulation and Analysis of a Three-Dimensional Finite Element Implementation for Adhesive Contact at the Nanoscale," Comput. Methods Appl. Mech. Eng., **198**(49–52), pp. 3871–3883.
[26] Sauer, R. A., 2011, "The Peeling Behavior of Thin Films With Finite Bending Stiffness and the Implications on Gecko Adhesion," J. Adhes., **87**(7–8), pp. 624–643.
[27] Lane, M., Dauskardt, R. H., Vainchtein, A., and Gao, H., 2000, "Plasticity Contributions to Interface Adhesion in Thin-Film Interconnect Structures," J. Mater. Res., **15**(12), pp. 2758–2769.
[28] Högberg, J. L., 2006, "Mixed Mode Cohesive Law," Int. J. Fract., **141**(3–4), pp. 549–559.
[29] Camanho, P. P., Davila, C. G., and de Moura, M. F., 2003, "Numerical Simulation of Mixed-Mode Progressive Delamination in Composite Materials," J. Compos. Mater., **37**(16), pp. 1415–1438.
[30] Williams, J. G., and Hadavinia, H., 2002, "Analytical Solutions for Cohesive Zone Models," J. Mech. Phys. Solids, **50**(4), pp. 809–825.
[31] Dugdale, D. S., 1960, "Yielding of Steel Sheets Containing Slits," J. Mech. Phys. Solids, **8**(2), pp. 100–104.